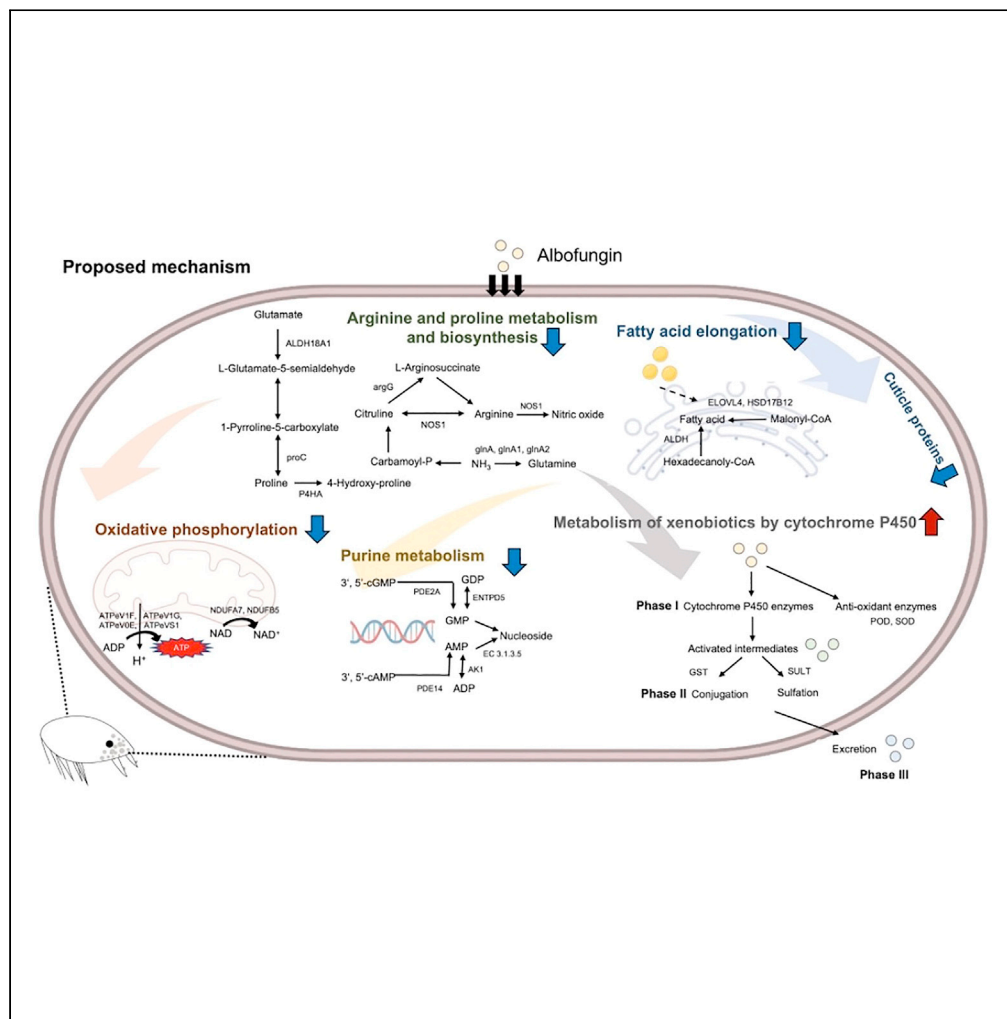


Article

Mode of action of antifouling compound albofungin in inhibiting barnacle larval settlement



Weiyi She, Hao Wang, Darwin Linardi, ..., Feng Chen, Aifang Cheng, Pei-Yuan Qian

chengaf@ust.hk (A.C.)
boqianpy@ust.hk (P.-Y.Q.)

Highlights

In situ hybridization revealed the spatial expression patterns of GST, NOS, and CaM

Albofungin affected energy and xenobiotic metabolisms in *A. amphitrite*

Providing insight into mechanisms of albofungin in inhibiting settlement of barnacle



Article

Mode of action of antifouling compound albofungin in inhibiting barnacle larval settlement

Weiyi She,^{1,2,3} Hao Wang,^{1,2} Darwin Linardi,⁴ Sin Yu Chik,^{1,2} Yi Lan,^{1,2} Feng Chen,⁵ Aifang Cheng,^{1,2,*} and Pei-Yuan Qian^{1,2,6,*}

SUMMARY

Marine biofouling causes huge economic losses to the marine industry every year. Albofungin is a potential antifoulant showing strong anti-macrofouling activities against larval settlement of major fouling organisms. In the present study, directed RNA-seq and proteomic analyses were used to investigate changes in the transcriptome and proteome of a major fouling barnacle *Amphibalanus amphitrite* cyprids in response to albofungin treatment. Results showed that albofungin treatment remarkably upregulated the metabolism of xenobiotics by the cytochrome P450 pathway to discharge the compound and downregulated energy metabolic processes. Intriguingly, immunostaining and whole-mount in situ hybridization (WISH) revealed the spatial expression patterns of selected differentially expressed genes (glutathione S-transferase [GST], nitric oxide synthase [NOS], and calmodulin [CaM]) distributed in the thorax and antennule of *A. amphitrite*. Our study provides new insights into the mechanism of albofungin in interrupting the larval settlement of *A. amphitrite* and suggests its potential application as an antifouling agent in marine environments.

INTRODUCTION

Biofouling refers to the accumulation of unwanted marine fouling organisms colonizing on man-made surfaces and causes substantial economic loss in the marine industry.¹ Biofoulers include microfoulers, such as marine bacteria and algae, and macrofoulers, such as barnacles, mussels, tubeworms, and bryozoans.² In the case of ships, the settlement of these biofoulers causes adverse effects, such as high frictional resistance and increase in the frequency of dry-docking operations.³ Among all different solutions throughout history, applying biocides, such as tributyltin (TBT), to marine coatings has been one of the successful ways to combat biofouling.⁴ However, the application of TBT on ships was banned due to its high toxicity.⁵ Other biocides, such as SeaNine 211, also have environmental pollution problems and toxicity toward non-target marine organisms, causing non-negligible harm to the marine ecosystem.⁶ Therefore, maritime industry needs green and safer antifouling agents desperately.

Marine natural products are readily biodegradable and environmentally friendly.⁷ Hundreds of antifoulants have been identified since 1995, and most of them were discovered through antilarval-settlement or antibiofilm bioassays.⁸ However, the underlying mode of actions of these antifoulants have rarely been investigated, limiting their translational application. Thus, it is important to examine the molecular mechanisms of antifouling compounds against their target biofoulers and their acute and chronic toxicity to nontarget organisms in order to develop antifouling compounds into commercial products.⁸ For example, butenolide, one of the representative commercialized antifoulants, is isolated from the marine bacterium *Streptomyces albidoflavus*; it can bind to acetyl-CoA acetyltransferase 1 (ACAT1) in barnacle *Amphibalanus amphitrite*, acyl-CoA dehydrogenase (ACADVL) and glutathione S-transferase (GST) in bryozoan *Bugula neritina*, and succinyl-CoA synthetase β subunit (SCS β) in the marine bacterium *Vibrio* sp.⁹

We previously isolated a series of albofungin derivatives from *Streptomyces chrestomyceticus* BCC 24770, and all the derivatives showed a broad spectrum of antibiofilm activities against both Gram-positive and Gram-negative bacteria.¹⁰ Albofungin also exhibited potent antilarval settlement activity against two major fouling organisms, the barnacle *A. amphitrite* and the bryozoan *B. neritina* in both lab and field tests and

¹Southern Marine Science and Engineering Guangdong Laboratory (Guangzhou), Nansha, Guangdong, China

²Department of Ocean Science and Hong Kong Brach of Southern Marine Science and Engineering Guangdong Laboratory (Guangzhou), Hong Kong University of Science and Technology, Hong Kong, China

³SZU-HKUST Joint PhD Program in Marine Environmental Science, Shenzhen University, Shenzhen 518060, China

⁴Chemical and Biological Engineering, Hong Kong University of Science and Technology, Hong Kong, China

⁵Institute for Advanced Study, Shenzhen University, Shenzhen 518060, China

⁶Lead contact

*Correspondence: chengaf@ust.hk (A.C.), boqianpy@ust.hk (P.-Y.Q.)

<https://doi.org/10.1016/j.isci.2023.106981>



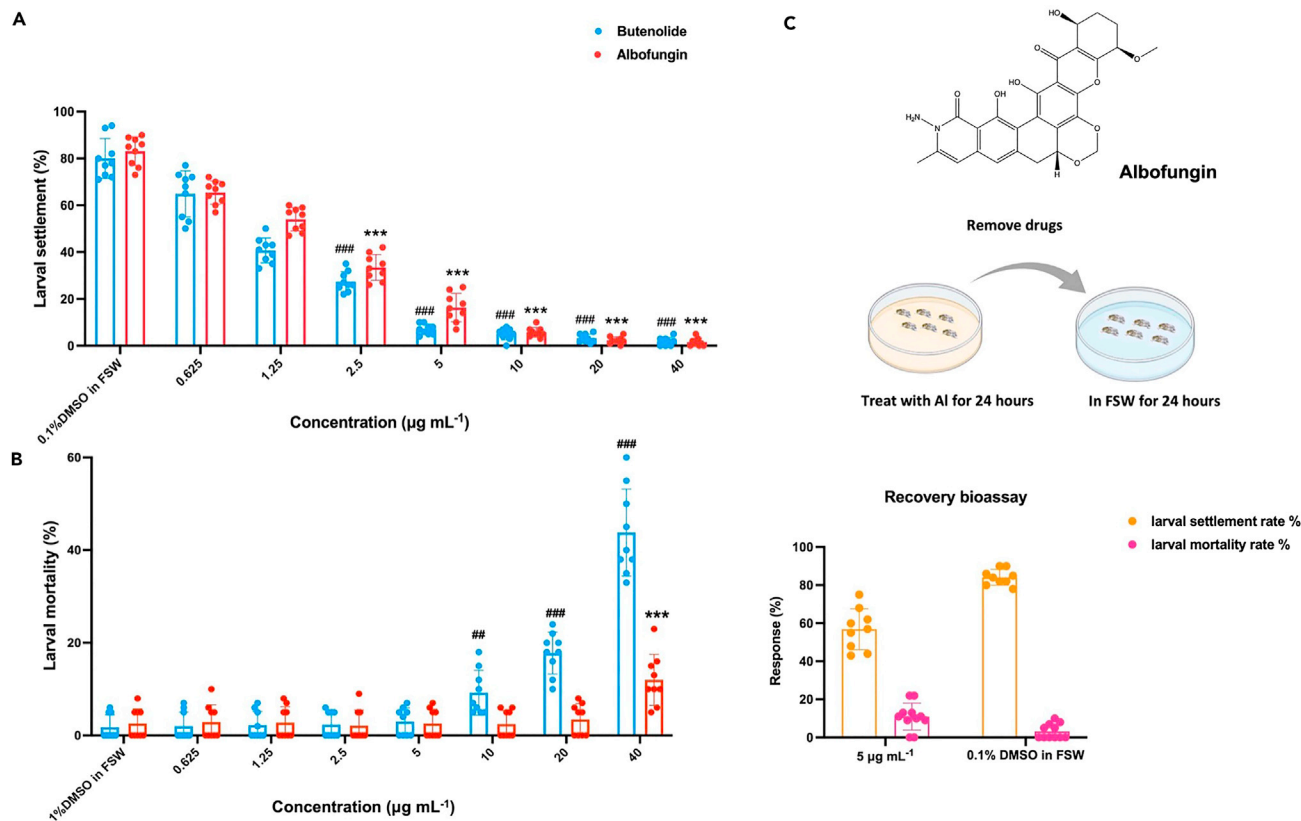


Figure 1. Larval settlement and mortality in different concentrations of albobungin treatment for 48 h

(A and B) Larval settlement rate (A) and larval mortality rate (B). 1% DMSO in FSW served as the negative control. Butenolide was used as the positive control. Error bars represent SD, $n = 9$. Significant differences were analyzed by one-way ANOVA compared with the control 0.1% DMSO in FSW, ## $p < 0.01$; ###, *** $p < 0.001$.

(C) Recovery bioassay of albobungin-treated cyprids. Error bars represent SD, $n = 9$. Significant differences were analyzed by one-way ANOVA compared with the control 0.1% DMSO in FSW.

its antilarval settlement performance was comparable with butenolide,¹⁰ indicating that albobungin is a promising antifouling reagent in maritime applications.

In the present study, we aim to examine the molecular mechanism of albobungin in inhibiting macrofoulers, using *A. amphitrite* as a model organism since barnacle attach firmly to man-made surfaces and are difficult to remove and thus, has been used as a model in biofouling related research.^{11,12} Barnacles have a complex life cycle, and their larvae go through six naupliar stages before transforming into the cyrid stage. During the cyrid stage, larvae search for a suitable place to attach and metamorphose into juveniles.¹³ Previous studies showed that the proteins in the nervous system, energy metabolic and signal transduction pathways participated in the cyrid attachment and metamorphosis,^{14–16} which paves the way for identifying the mode of action of antifouling compounds. In the present study, we used transcriptomics and proteomics to elucidate the changes in metabolic pathways of *Amphibalanus amphibalanus* after albobungin exposure. Furthermore, we compared the transcriptome profiles of *A. amphibalanus* between albobungin and butenolide treatment to gain more insight into the mode of action of albobungin.

RESULTS AND DISCUSSION

Albobungin inhibited larval settlement potently and reversibly

The effect of albobungin on larval settlement activity and mortality of *A. amphitrite* were measured. After incubation for 48 h, the larval settlement rate was significantly reduced to $33.4\% \pm 5.5\%$ at $2.5 \mu\text{g mL}^{-1}$ albobungin treatment compared with the 0.1% DMSO control group ($83.1\% \pm 6.1\%$, Figure 1A). Among all treatment groups, albobungin inhibited larval settlement in a dose-dependent manner. Larvae in the

albofungin treatment groups exhibited relatively slower swimming velocity than those in the control group. The cytotoxicity of albofungin was evaluated by calculating the mortality rate after incubation for 48 h; the highest mortality rate of 40 $\mu\text{g mL}^{-1}$ albofungin was 12% \pm 5.5%, which was lower than the butenolide treatment group (43.7% \pm 9.4%, [Figure 1B](#)).

The recovery assay was conducted to determine whether the cyprids would attach and normally metamorphose after exposure to albofungin. After replacing the albofungin solution with FSW within 24 h, 57% (\pm 10.8%) of cyprids were able to recover from the albofungin treatment, and only 11% (\pm 7.1%) of cyprids died after the treatment ([Figure 1C](#)). Hence, the effect of albofungin on settling cyprids was largely reversible.

Proteomics analysis of *A. amphitrite* upon albofungin treatment

Mass spectrometry-based quantitative proteomics of *A. amphitrite* was performed to identify the mode of action of albofungin. A total of 224 differentially expressed proteins (DEPs) were identified when proteomes between the albofungin treatment group and the control group were compared. The volcano plots of fold changes against p values indicated that the proteins in the cyprids with different expression levels in the absence and presence of albofungin, and in response to albofungin treatment, the expression of proteins was more downregulated than upregulated ([Figure 2A](#)). The principal component analysis (PCA) indicated that the albofungin-treated group and the control group were well separated ([Figure S1](#)).

The full list of DEPs is shown in [Table S3](#). The Kyoto Encyclopedia of Genes and Genomes (KEGG) enrichment analyses showed that after albofungin treatment, the expression levels of proteins in the metabolism of xenobiotics by the cytochrome P450 pathway (e.g., glutathione S-transferase-like, cytochrome P450 3A31-like), autophagy and mitophagy-related proteins (ras-related protein M-Ras-like isoform X1, sequestosome-1-like isoform X1, cathepsin D-like), and two peroxidases were significantly increased, whereas the expression of proteins in various metabolic pathways including arginine biosynthesis and metabolism (e.g., glutamine synthetase-like, ornithine aminotransferase, arginine kinase), oxidative phosphorylation (ATP synthase subunit delta mitochondrial-like, V-type proton ATPase subunit d, cytochrome c oxidase subunit 6C-like), and mismatch repair (replication factor C subunit 3-like) were significantly reduced ([Figures 2B and 2C](#)). Moreover, albofungin significantly decreased the expression of a number of cuticle proteins.

Transcriptome profiling upon albofungin treatment

To reinforce our proteomics data, we further performed the transcriptomic analysis of the cyprids treated with 5 and 20 $\mu\text{g mL}^{-1}$ albofungin. A total of 262,413,305 reads were obtained from 12 samples (three replicates each in the control group, 5 $\mu\text{g mL}^{-1}$ albofungin treatment group, 20 $\mu\text{g mL}^{-1}$ albofungin treatment group, and 5 $\mu\text{g mL}^{-1}$ butenolide treatment group) and mapped these reads to the reference barnacle *A. amphitrite* transcriptome containing 65,305 transcripts from NCBI (RefSeq GCF_019059575.1). The Benchmarking Universal Single-Copy Orthologs (BUSCO) assessment results showed 92.5% completeness for the assembled transcriptome. A total of 42,833 genes were annotated in Gene Ontology (GO), 37,915 in the KEGG, and 51,916 in Eukaryotic Orthologous Groups (KOG).

The expression level of each gene in the control, albofungin treatment, and butenolide treatment groups was then calculated. Using the gene expression data (transcripts per million [TPM] value), the PCA plots were made, which showed a clear separation between the control group and the high- and low-concentration albofungin treatment groups with a 55% variance on two PCs ([Figure 3A](#)). However, some variability among the replicates within the same group was detected, which shall be acceptable because *A. amphitrite* adult samples obtained in the wild environment might result in individual variations. Moreover, in [Figure 3B](#), PC1 suggested that the extent of similarity between the albofungin-treated group and the control group was higher than that between the butenolide-treated group and the control group, which suggested clearly different mode of anti-larval settlement action between albofungin and butenolide. The volcano plots of fold changes against p values along with 1,852 and 1,819 differentially expressed genes (DEGs) were identified in the 5 and 20 $\mu\text{g mL}^{-1}$ albofungin treatment groups compared with the control group ([Figures 3C and 3D](#)). Furthermore, the Venn diagram showed that 690 upregulated DEGs and 500 downregulated DEGs overlapped in the albofungin treatment groups ([Figure S2](#)).

To investigate the biological activities and metabolic pathways in *A. amphitrite* influenced by albofungin treatment, the identified DEGs were further subjected to KOG and GO analyses and KEGG pathways

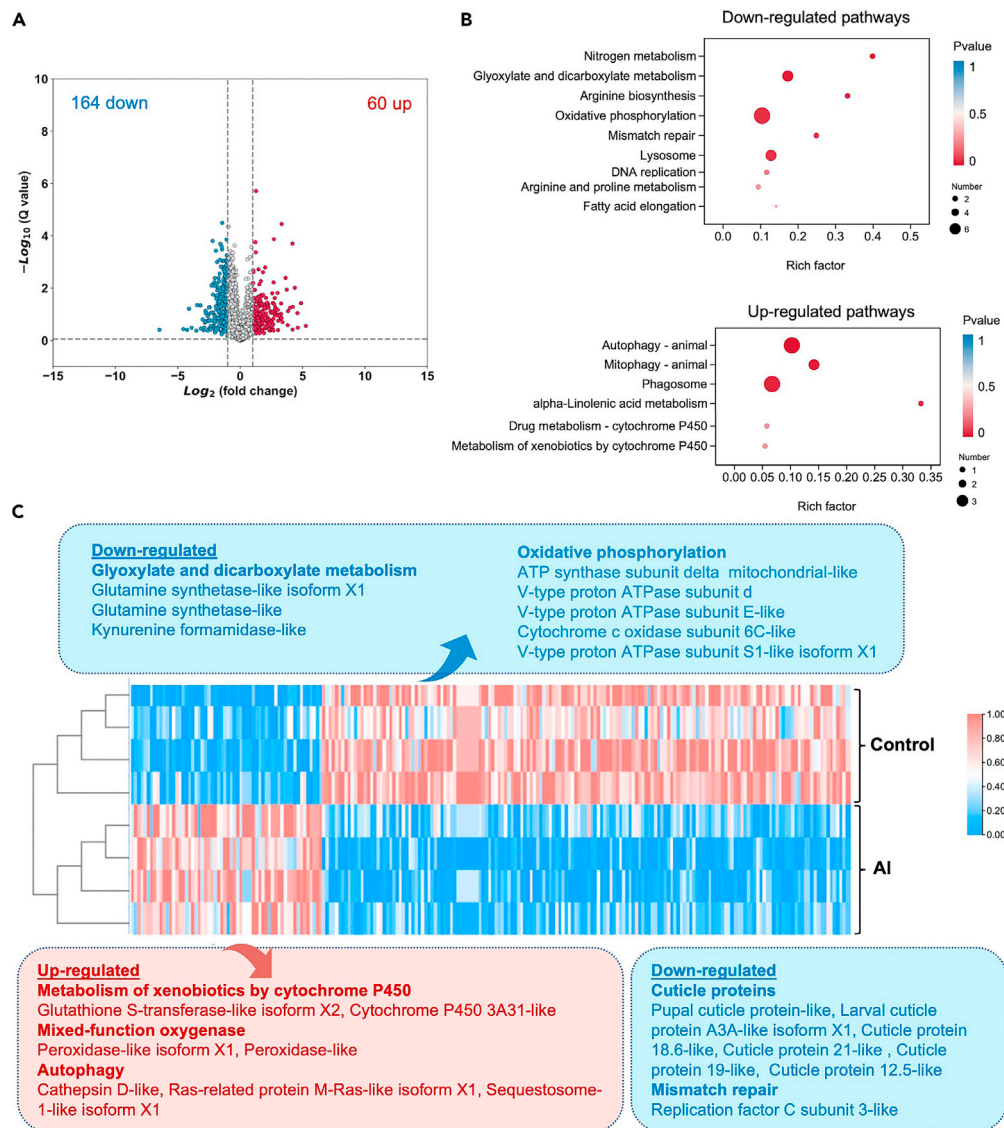


Figure 2. Proteomics analysis of *A. amphitrite* upon albofungin treatment

(A) Volcano plots of the cyprids upon albofungin treatment compared with those before treatment. Upregulated proteins are those with higher expression levels in the albofungin-treated cyprids (shown in red spots), while downregulated proteins are those with lower expression levels in the albofungin-treated cyprids (shown in blue spots).

(B) KEGG enriched pathways of the differentially expressed proteins (DEPs) after albofungin treatment. In each inset, the Y axis is the enriched KEGG pathway, and the X axis is the Rich factor, which is the ratio of the number of DEPs annotated in a pathway to all annotated proteins. The diameter of each dot represents the number of proteins annotated to the KEGG pathway, and the color scale represents the *p*-value of the enrichment.

(C) Heatmap of expression level (label-free quantification [LFQ] intensity) of the DEPs across all groups. The upregulated and downregulated processes after albofungin treatment and identities of some DEPs are listed up or below the heatmap.

enrichment analysis (Figures 3, S3, and S4), which led to 810 out of 42,833 annotated genes being assigned to three major GO functional categories: "biological process," "cellular component," and "molecular function," which included 20, 15, and 11 functional classes, respectively (Figure S3). The KEGG-enriched pathways of all the DEGs showed a similar pattern between the high-concentration group ($20 \mu\text{g mL}^{-1}$ albofungin treatment) and the low-concentration group ($5 \mu\text{g mL}^{-1}$ albofungin treatment), along with the PCA analysis, suggesting that the high and low concentrations of albofungin treatment groups caused a similar trend of actions in the larval metabolic pathways. A list of DEGs with the expression level and

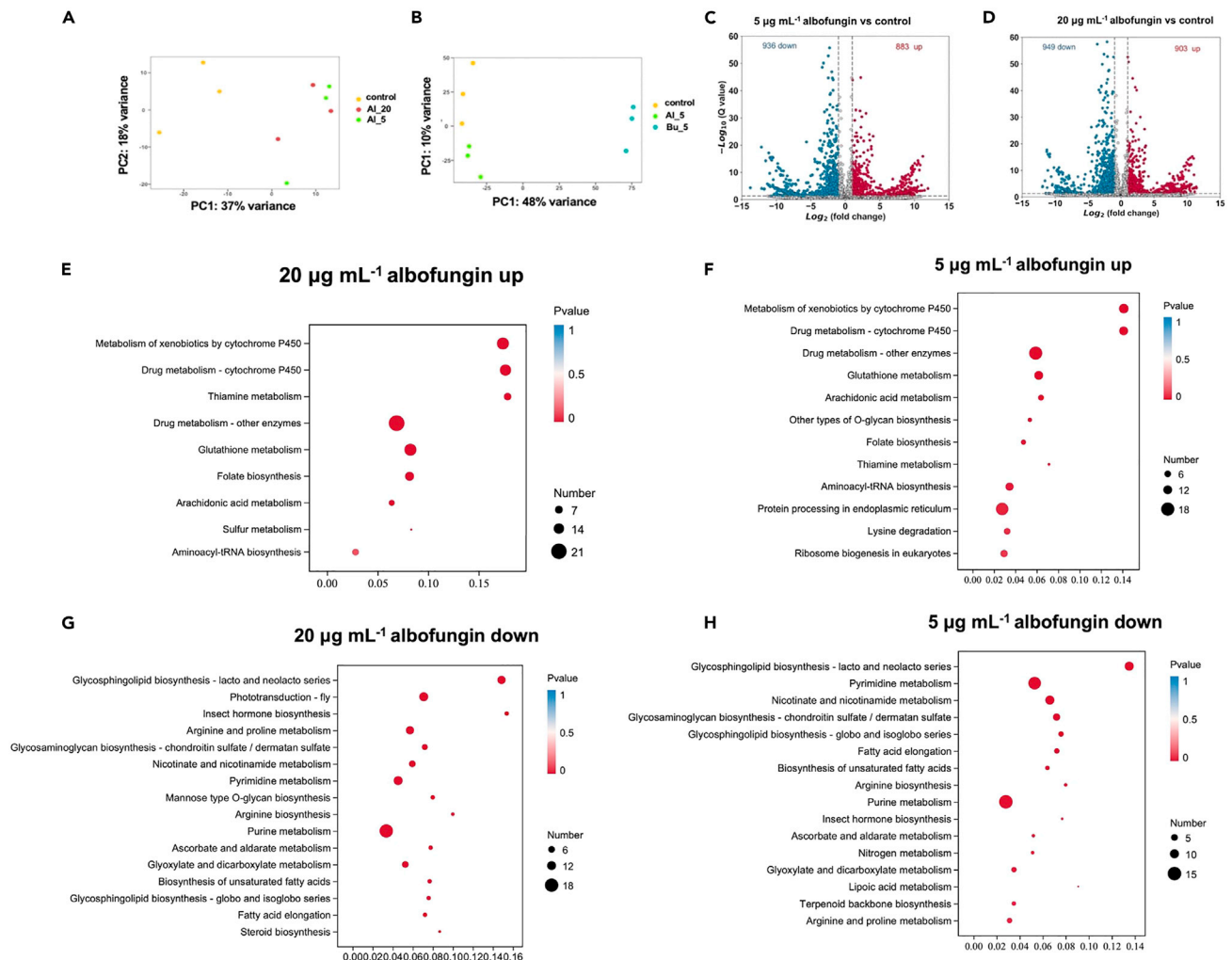


Figure 3. Transcriptomic analysis of *A. amphitrite* larvae in response to albofungin treatment

(A) Principal component analysis (PCA) results based on gene expression levels of the albofungin-treated group and control group. (B) PCA results based on gene expression levels of albofungin-treated group (5 $\mu\text{g mL}^{-1}$), butenolide-treated group (5 $\mu\text{g mL}^{-1}$), and control group. (C and D) Volcano plots of albofungin-treated groups (5 $\mu\text{g mL}^{-1}$ and 20 $\mu\text{g mL}^{-1}$) compared with the control group. Upregulated genes are those with higher expression levels in the albofungin-treated cyprids (shown in red spots), while downregulated genes are those with lower expression levels in the albofungin-treated cyprids (shown in blue spots). (E and F) KEGG-enriched upregulated pathways after 20 $\mu\text{g mL}^{-1}$ albofungin (E) or 5 $\mu\text{g mL}^{-1}$ albofungin (F) treatment. (G and H) KEGG-enriched downregulated pathways after 20 $\mu\text{g mL}^{-1}$ albofungin (G) or 5 $\mu\text{g mL}^{-1}$ albofungin (H) treatment. In each inset, the Y axis is the enriched KEGG pathway, and the X axis is the Rich factor, which is the ratio of the number of differentially expressed genes (DEGs) annotated in a pathway to all annotated genes. The diameter of each dot represents the number of genes annotated to the KEGG pathway, and the color scale represents the *p*-value of the enrichment.

fold change to the corresponding pathways is presented in Table S4. The pairwise comparison between 5 and 20 $\mu\text{g mL}^{-1}$ albofungin treatment groups and the control group showed that the pathways of “metabolism of xenobiotics by cytochrome P450” (ko00980) and “glutathione metabolism” (ko00480) were significantly upregulated, whereas “srginine and proline metabolism” (ko00330), “fatty acid elongation” (ko00062), “pyrimidine metabolism” (ko00240), and “purine metabolism” (ko00230) were significantly downregulated (Figure 3).

Upregulated metabolism of xenobiotics by cytochrome P450 in response to albofungin treatment

Remarkably, 12 genes encoding for GST were highly enriched in the top 20 KEGG pathways of “metabolism of xenobiotics by cytochrome P450” and “glutathione metabolism” in the 5 and 20 $\mu\text{g mL}^{-1}$ albofungin

treatment groups (Figures 3E and 3F). More specifically, *trans*-1,2-dihydrobenzene-1,2-diol dehydrogenase-like isoform X3 (DHDH) was 7.3- to 8.8-fold higher than that in the control group, and GST 1-like (GST) was 3.5- and -3'.4-fold higher than that in the control group in the pathway of metabolism of xenobiotics by CYP. To determine the influence of albofungin on other gene expressions in the detoxification process and antioxidant enzyme activities, the gene expression levels of the mixed-function oxygenase (MFO) system components and detoxification enzymes were further checked. Intriguingly, 19 CYPs, 7 sulfotransferases (SULTs), 1 superoxide dismutase (SOD), and 1 PX were significantly upregulated in the albofungin treatment groups (Table S4). Similarly, various GST genes were significantly upregulated in the butenolide treatment group from 1.2- to 9.0-folds, respectively. We further analyzed the stress-related genes and found that one heat shock 70 kDa protein was upregulated only in the 5 $\mu\text{g mL}^{-1}$ albofungin treatment group and heat shock protein (HSP) 60A-like and heat shock 70 kDa protein Ab-like were upregulated only in the 20 $\mu\text{g mL}^{-1}$ albofungin treatment group. However, in the butenolide treatment group, more HSPs, such as heat shock 70 kDa protein, heat shock 90 kDa protein, and HSP 60 were upregulated by 1.0- to 21.7-folds (Table S5).

GSTs have various biological functions, such as cell protection against oxidative stresses and toxic molecules.¹⁷ Most importantly, GSTs participate in phase II of cell detoxification processes to generate hydrophilic compounds that can be easily excreted.¹⁸ Other phase II detoxification enzymes include SULTs, which are involved in the metabolism of xenobiotics, such as quinolones and amino drugs.¹⁹ In the phase I reaction, multiple CYP enzymes are employed mainly in hydroxylation and act as monooxygenases, dioxygenases, and hydrolases.²⁰ Thus, the two phases constitute the primary process for the biotransformation of xenobiotics.²¹ The results in the present study indicated that when the larvae were exposed to albofungin, the high expression levels of SOD, PX, CYPs, SULTs, DHDH, and GSTs can be used to oxidize compounds to become more susceptible to metabolism and excretion as well as to produce an efflux of xenobiotics from the cells. The expression of HSP family proteins is very sensitive to stress;²² the HSP70 levels are altered in larvae in response to several antifouling compounds.^{13,23} The high expression levels of HSPs in the butenolide treatment group but not in albofungin treatment groups indicated that butenolide might act on these proteins while albofungin may not.

Downregulation of genes related to fatty acid elongation, arginine biosynthesis and metabolism, and oxidative phosphorylation in response to albofungin treatment

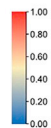
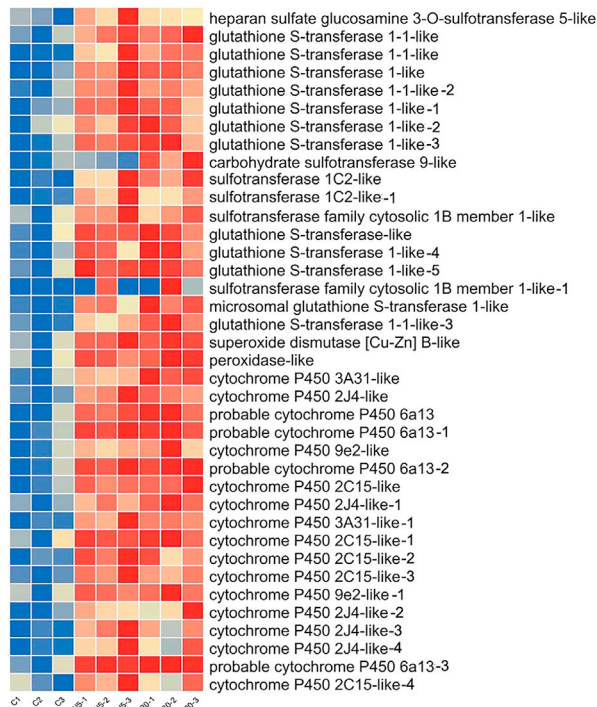
The KEGG enrichment analysis highlighted the significantly downregulated pathways of "fatty acid elongation" and "arginine and proline metabolism" (Figures 3G and 3H). The genes in the fatty acid elongation, including elongation of very long chain fatty acids protein 1-like (ELOVL1, 4.1- and 5.0-folds in the 5 $\mu\text{g mL}^{-1}$ and 20 $\mu\text{g mL}^{-1}$ albofungin treatment groups compared with the control group), elongation of very long chain fatty acids protein 7-like (ELOVL7, 3.0- and 3.3-fold in the 5 and 20 $\mu\text{g mL}^{-1}$ albofungin treatment groups compared with the control group), and three very-long-chain 3-oxoacyl-CoA reductase-like genes were significantly downregulated in 5 and 20 $\mu\text{g mL}^{-1}$ albofungin treatment groups (Table S4). Genes involved in arginine and proline metabolism and arginine biosynthesis pathways were significantly downregulated, such as *glnA*, argininosuccinate synthase (*argG*), and prolyl 4-hydroxylase subunit alpha-1-like (*P4HA*) genes (Figure 4). In particular, aldehyde dehydrogenase family 3 member B1-like (*ALDH*), 4-hydroxy-2-oxoglutarate aldolase (*HOGA1*), and pyrroline-5-carboxylate reductase 3-like (*proC*) genes were significantly downregulated by 22.3, 23.0, and 7.8-fold in the 20 $\mu\text{g mL}^{-1}$ albofungin treatment group compared with those in the control group. In contrast, changes of these genes in the expression level in the 5 $\mu\text{g mL}^{-1}$ albofungin treatment group were not significant, indicating that treatment with high concentration will inhibit arginine and proline metabolism and arginine biosynthesis. Furthermore, several V-type proton ATPase and NADH (nicotinamide adenine dinucleotide) dehydrogenase genes involved in the oxidative phosphorylation pathway were downregulated in both albofungin treatment groups by up to 22-folds compared with those in the control group.

Cyprids rely on stored lipids and proteins as primary energy sources to swim and metamorphosis because they do not feed.²⁴ During the early cyprid development stage, energy- and metabolism-related proteins were upregulated, which played an essential role in the larval settlement of barnacles.¹⁶ As previously reported, butenolide was bound to the ACAT1 in *A. amphitrite*, which participated in ketone body metabolism.⁹ Similar to butenolide, albofungin showed an inhibitive effect on energy production. Two elongations of very long chain fatty acids proteins (ELOVL1 and ELOVL7) were significantly downregulated in fatty acid metabolism in both treatment groups with significant fold changes. ELOVL1 catalyzes the first

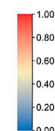
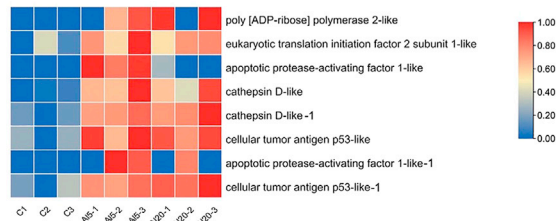
A

Upregulated

Metabolism of xenobiotics by cytochrome P450 and MFO system



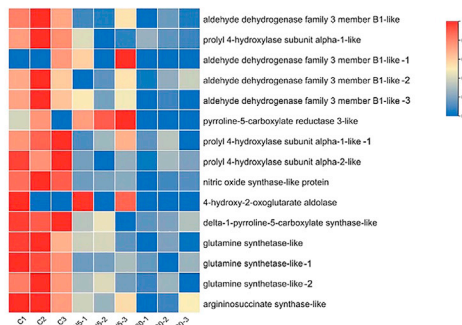
Apoptosis, p53 signaling pathway



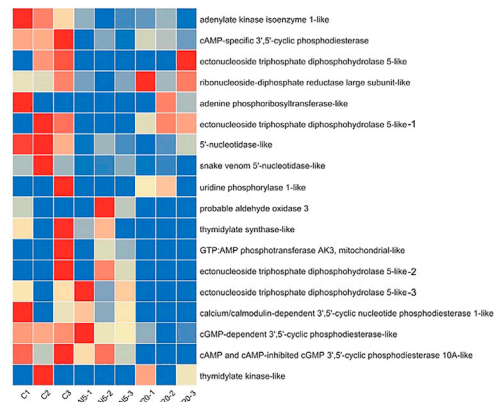
B

Downregulated

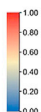
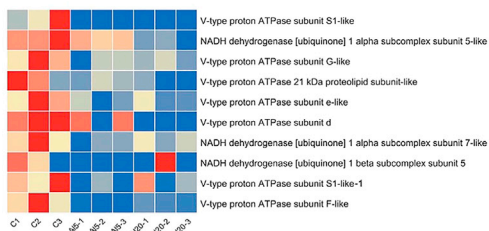
Arginine and proline metabolism and biosynthesis



Purine and pyrimidine metabolism



Oxidative phosphorylation



Fatty acid elongation

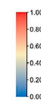
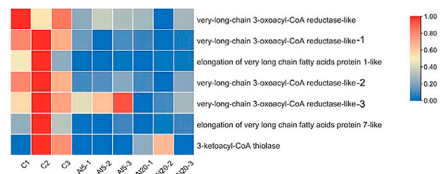


Figure 4. Heat map of expression level (TPM) of the upregulated and downregulated pathways upon albobfungin treatment

(A and B) Upregulated (A) and downregulated (B) genes from selected KEGG pathways on the cyprids between the albobfungin treatment group and the control group.

reaction, which is rate-limiting among the four reactions that constitute the long-chain fatty acids elongation cycle.²⁵ In the oxidative phosphorylation process, the downregulated V-ATPases acidify intracellular organelles and their plasma membranes, combining the energy of ATP hydrolysis with proton transport.²⁶ We here found here that the energy-related pathways were significantly downregulated after albobfungin treatment, indicating that albobfungin negatively regulated energy metabolism in the larval settlement.

Upregulated P53 signaling pathway in response to albobfungin treatment

Two cellular tumor antigen p53-like, two apoptotic protease-activating factor 1-like, and two cathepsin D-like genes were significantly upregulated in the 5 and 20 $\mu\text{g mL}^{-1}$ albobfungin treatment groups (Figure 4A). The TP53 gene is a cellular sensor for DNA damage and therefore protects the cell by responding to cellular insults by inducing cell-cycle arrest or apoptosis. The other downregulated cytosolic cathepsins D are implicated in the degradation of bid in the apoptosis, resulting in its activation and translocation to mitochondria. As previously reported, albobfungin activated the apoptosis pathway in HeLa cells,²⁷ suggesting that it may exhibit a negative impact on the fouling organisms.

Downregulation of purine and pyrimidine metabolism and cuticle genes in response to albobfungin treatment

Purine and pyrimidine metabolism and DNA replication pathways were significantly downregulated after albobfungin treatment. The deregulation of DEGs involved in the pathways, such as 5'-nucleotidase-like (5NT), adenylate kinase (AK), and ectonucleoside triphosphate diphosphohydrolase 5 (ENTPD5), DNA polymerase epsilon catalytic subunit A-like (POLE), and DNA mismatch repair protein Mlh1-like isoform X2 (MLH1), indicated that albobfungin may disrupt the synthesis and degradation of purine nucleotides and DNA replication processes (Figure 4B). A number of cuticle proteins (e.g., cuticle protein AMP4-like, cuticle protein 7-like) were also downregulated by 3.3- and 4.1-folds in the 20 $\mu\text{g mL}^{-1}$ albobfungin treatment group. In the premolt period, cyprid larvae partly resorb their old cuticles to prepare for new cuticles. Thus, the downregulated cuticle proteins might affect the molting cycles of larvae.²⁸ Defection of purine nucleotide metabolism in silkworms causes a translucent larval integument and male infertility.²⁹ During barnacle metamorphosis, the morphology is altered dramatically, so the processes of cell apoptosis, proliferation, and differentiation are involved.³⁰ Therefore, the decreased purine metabolism after albobfungin treatment may cause larval development defection.

WISH and qPCR analysis of the expression patterns of selected DEGs

To validate the RNA-Seq results, we selected some DEGs involved in arginine biosynthesis, purine metabolism, fatty acid elongation, oxidative phosphorylation, metabolism of xenobiotics by CYP, and other genes (calmodulin [CaM], POD, and CTSD) for qRT-PCR analysis (Figure 5). The results showed that CTSD, CYP2J4, POD, CYP2C15, and GST1 genes were upregulated by 1.5–4.3-folds in the 5 $\mu\text{g mL}^{-1}$ albobfungin treatment group and by 2.8–8.5-folds in the 20 $\mu\text{g mL}^{-1}$ albobfungin treatment group (Figure 5A). In contrast, HSD17B12, NOS1, GPCR, glnA, 5'-NT, CaM, and V-ATPase genes were downregulated in both groups (Figure 5B). Generally, most of the qRT-PCR results of the selected genes were consistent with the RNA-Seq results, indicating the reliability of the RNA-Seq data.

Among the DEGs, we examined the spatial pattern of CaM, GST, and nitric oxide synthase (NOS) genes, which are involved in larval settlement.^{13,31,32} The presence of CaM, GST, and NOS transcripts was detected by DIG-labeled antisense RNA probes (Table S2). An overall picture of the immunostaining and different stages of larvae is shown in Figures 6A and 6B, which indicated the muscle fibers and cilia location in the cyprids. Whole-mount *in situ* hybridization (WISH) of cyprids showed that CaM transcript was expressed in the muscle fiber-rich thorax and the pairs of antennules (Figure 6C). The expression pattern of the NOS transcript was the same as observed in CaM mainly in the antennule and thorax, consistent with the previous report that NOS is present in settlement-critical structures, such as muscles and cement glands,³³ whereas the GST transcript was detected only in the thorax with a strong signal, consisting of muscle fibers.

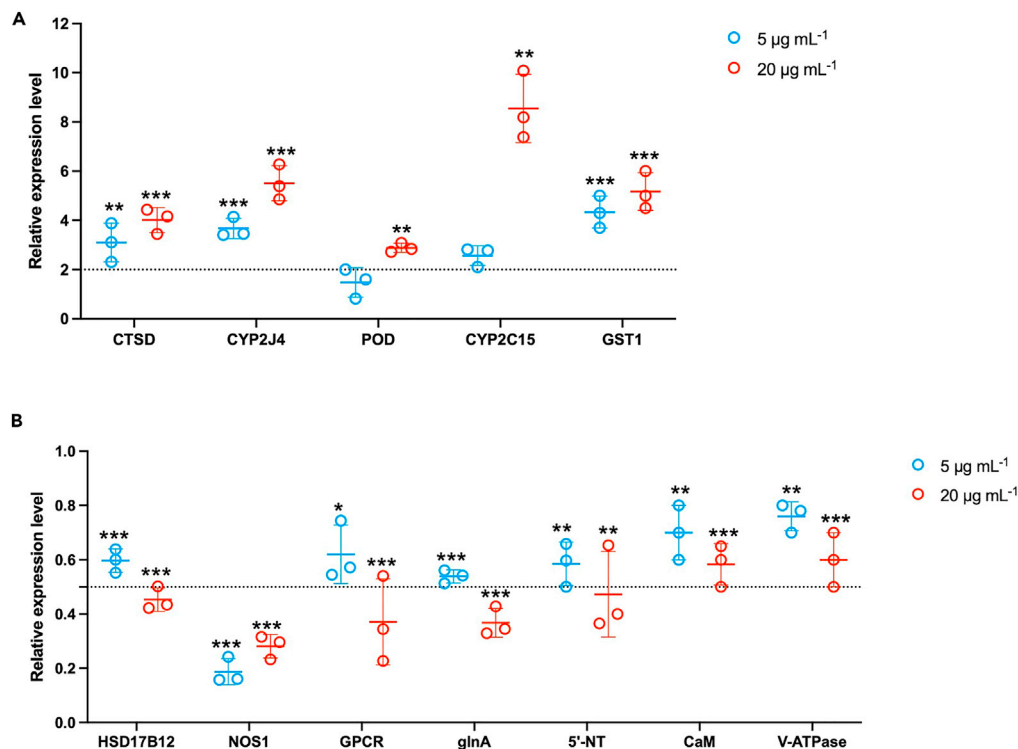


Figure 5. Real-time PCR results of the gene expression level of selected differentially expressed genes (DEGs) upon albufungin treatment

(A and B) Upregulation of the selected DEGs (A) and downregulation of the selected DEGs (B) after albufungin treatment. The data represent mean \pm SD ($n = 3$). Significant differences were analyzed by one-way ANOVA compared with the control, * $p < 0.05$, ** $p < 0.01$, *** $p < 0.001$.

CaM activates various Ca²⁺-dependent enzyme reactions along with binding to CaM-binding proteins, including phosphatases, NOS, and G-protein coupled receptors to regulate cellular bioactivities,^{31,34,35} such as muscle contraction, cell division, and differentiation.³⁶ In the previous report, CaM had higher expression in the cyprid stage than VI nauplii and juvenile stages, and the CaM inhibitor compound 48/80 effectively inhibited barnacle larval settlement.³¹ Thus, the significant downregulation of the CaM genes and the inactive larval movement indicated that CaM may be the potential target of the compound for limiting larval locomotion. Nitric oxide (NO) acts as a negative signal transduction molecule and the NO/cGMP signaling pathway can inhibit *A. amphitrite* larva settlement.^{23,32,37} NOS and soluble guanylyl cyclase (sGC) inhibitors promote the settlement of *A. amphitrite* larvae.³⁷ However, in our dataset of the albufungin-treated transcriptome, the NOS gene was significantly downregulated by 1-fold, but the sGC gene was not differentially expressed upon treatment with 5 or 20 $\mu\text{g mL}^{-1}$ albufungin, indicating that the albufungin treatment might not target on the NO/cGMP signaling pathway.

According to our previous study, albufungin exhibited potent anti-larval settlement activity against *A. amphitrite* larvae.¹⁰ Treatment with 5 $\mu\text{g mL}^{-1}$ albufungin exerted a recoverable and short-term inhibitory effect on the larval settlement of *A. amphitrite* in the present study. In general, antifouling compounds with specific molecular targets, such as pathways or enzymes that regulate energy metabolism, are often considered non-toxic, whereas those that do not target any specific molecular targets can be toxic.¹ Hence, albufungin showed dose-dependent anti-larval settlement activity, and the detailed transcriptome analysis revealed the positive correlation between albufungin concentrations and gene expression levels, suggesting that albufungin could target several specific biological processes and may thereby be considered non-toxic.

To conclude, the present study demonstrated that albufungin exhibited potent and reversible antifouling activity and the potential mode of action in *A. amphitrite* was mainly related to energy and xenobiotic

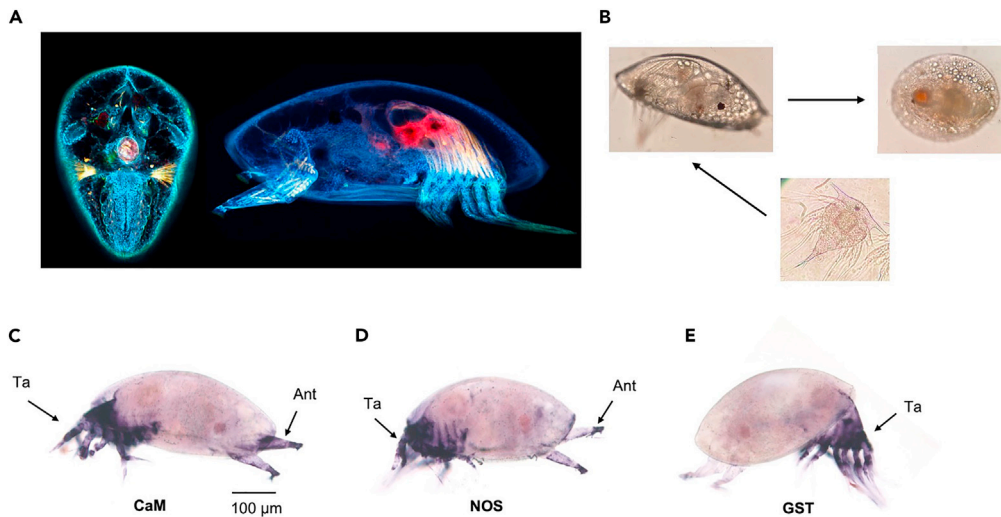


Figure 6. Gene spatial expression pattern of *A. amphitrite*
(A) Immunostaining of the whole cyprid. Yellow: muscle fibers, red: cilia.
(B) Developmental stages of the barnacle *Amphibalanus amphitrite*.
(C–E) Gene spatial expression pattern of (C) *CaM*, (D) *NOS*, and (E) *GST* genes.

metabolism by CYP pathways. A better understanding of the mode of action of albofungin in fouling organisms is necessary for its further development and potential in antifouling applications.

Limitations of the study

In the present study, transcriptomics and proteomics were used to investigate albofungin's action on barnacles, which provides the possible target biological pathways. These molecular targets could be further verified through genetic and/or biochemical manipulation experiments. Moreover, it is important to determine the adverse effects of albofungin on non-target organisms as well as how it degrades in marine environments before it can be commercially available.

STAR★METHODS

Detailed methods are provided in the online version of this paper and include the following:

- [KEY RESOURCES TABLE](#)
- [RESOURCE AVAILABILITY](#)
 - Lead contact
 - Materials availability
 - Data and code availability
- [EXPERIMENTAL MODEL AND SUBJECT DETAILS](#)
 - Larval collection and culture
- [METHOD DETAILS](#)
 - Larval bioassays
 - Sample preparation for proteomics
 - RNA sample preparation and sequencing
 - Transcriptome assembly and annotation
 - qPCR analysis
 - *In situ* hybridization
- [QUANTIFICATION AND STATISTICAL ANALYSIS](#)
 - Database searching and label-free quantification (LFQ) of proteomics data
 - Gene expression and enrichment analysis
 - Quantification of gene expression level from qPCR
 - Statistical analysis

SUPPLEMENTAL INFORMATION

Supplemental information can be found online at <https://doi.org/10.1016/j.isci.2023.106981>.

ACKNOWLEDGMENTS

The authors are thankful for the financial support from the Major Project of Basic and Applied Basic Research of Guangdong Province (2019B030302004), Southern Marine Science and Engineering Guangdong Laboratory (Guangzhou) (2021HJ01, SMSEGL20SC01), and the Research Grants Council of Hong Kong (C6026-19G-A and 16101822).

AUTHOR CONTRIBUTIONS

W.S. and H.W.: Conceptualization. W.S.: Formal analysis and writing—original draft. A.C., H.W., and P.-Y.Q.: Writing—review and editing. W.S., H.W., L.D., C.S.Y., and Y.L.: Investigation. F.C., P.-Y.Q., and A.C.: Project administration. P.-Y.Q.: Funding acquisition. All authors contributed to the article and approved the submitted version.

DECLARATION OF INTERESTS

The authors declare no competing interests.

Received: January 4, 2023

Revised: March 6, 2023

Accepted: May 24, 2023

Published: May 28, 2023

REFERENCES

1. Qian, P.Y., Chen, L., and Xu, Y. (2013). Mini-review: molecular mechanisms of antifouling compounds. *Biofouling* 29, 381–400. <https://doi.org/10.1080/08927014.2013.776546>.
2. Bixler, G.D., and Bhushan, B. (2012). Biofouling: lessons from nature. *Philos. Trans. Royal Soc. A* 370, 2381–2417. <https://doi.org/10.1098/rsta.2011.0502>.
3. Cao, S., Wang, J., Chen, H., and Chen, D. (2011). Progress of marine biofouling and antifouling technologies. *Chin. Sci. Bull.* 56, 598–612. <https://doi.org/10.1007/s11434-010-4158-4>.
4. Yebra, D.M., Kil, S., and Dam-Johansen, K. (2004). Antifouling technology—past, present, and future steps towards efficient and environmentally friendly antifouling coatings. *Prog. Org. Coating* 50, 75–104. <https://doi.org/10.1016/j.porgcoat.2003.06.001>.
5. Antizar-Ladislao, B. (2008). Environmental levels, toxicity and human exposure to tributyltin (TBT)-contaminated marine environment. *Environ. Int.* 34, 292–308. <https://doi.org/10.1016/j.envint.2007.09.005>.
6. Chen, L., and Lam, J.C.W. (2017). SeaNine 211 as antifouling biocide: a coastal pollutant of emerging concern. *J. Environ. Sci.* 61, 68–79. <https://doi.org/10.1016/j.jes.2017.03.040>.
7. Liu, L.L., Wu, C.H., and Qian, P.Y. (2020). Marine natural products as antifouling molecules—a mini-review (2014–2020). *Biofouling* 36, 1210–1226. <https://doi.org/10.1080/08927014.2020.1864343>.
8. Wang, K.L., Wu, Z.H., Wang, Y., Wang, C.Y., and Xu, Y. (2017). Mini-review: antifouling natural products from marine microorganisms and their synthetic analogs. *Mar. Drugs* 15, 266. <https://doi.org/10.3390/md15090266>.
9. Zhang, Y.F., Zhang, H., He, L., Liu, C., Xu, Y., and Qian, P.Y. (2012). Butenolide inhibits marine fouling by altering the primary metabolism of three target organisms. *ACS Chem. Biol.* 7, 1049–1058. <https://doi.org/10.1021/cb200545s>.
10. She, W., Ye, W., Cheng, A., Ye, W., Ma, C., Wang, R., Cheng, J., Liu, X., Yuan, Y., Chik, S.Y., et al. (2022). Discovery, yield improvement, and application in marine coatings of potent antifouling compounds albobungins targeting multiple fouling organisms. *Front. Microbiol.* 13, 906345. <https://doi.org/10.3389/fmicb.2022.906345>.
11. Holm, E.R. (2012). Barnacles and biofouling. *Integr. Comp. Biol.* 52, 348–355. <https://doi.org/10.1093/icb/ics042>.
12. Han, Z., Sun, J., Zhang, Y., He, F., Xu, Y., Matsumura, K., He, L.S., Qiu, J.W., Qi, S.H., and Qian, P.Y. (2013). iTRAQ-based proteomic profiling of the barnacle *Balanus amphitrite* in response to the antifouling compound meleagrin. *J. Proteome Res.* 12, 2090–2100. <https://doi.org/10.1021/pr301083e>.
13. Zhang, Y., Xu, Y., Arellano, S.M., Xiao, K., and Qian, P.Y. (2010). Comparative proteome and phosphoproteome analyses during cyprid development of the barnacle *Balanus* (= *Amphibalanus*) *amphitrite*. *J. Proteome Res.* 9, 3146–3157. <https://doi.org/10.1021/pr1000384>.
14. Al-Aqeel, S., Ryu, T., Zhang, H., Chandramouli, K.H., and Ravasi, T. (2016). Transcriptome and proteome studies reveal candidate attachment genes during the development of the barnacle *Amphibalanus amphitrite*. *Front. Mar. Sci.* 3, 171. <https://doi.org/10.3389/fmars.2016.00171>.
15. Chandramouli, K.H., Al-Aqeel, S., Ryu, T., Zhang, H., Seridi, L., Ghosheh, Y., Qian, P.Y., and Ravasi, T. (2015). Transcriptome and proteome dynamics in larvae of the barnacle *Balanus Amphitrite* from the Red Sea. *BMC Genom.* 16, 1063–1117. <https://doi.org/10.1186/s12864-015-2262-1>.
16. Chen, Z.F., Zhang, H., Wang, H., Matsumura, K., Wong, Y.H., Ravasi, T., and Qian, P.Y. (2014). Quantitative proteomics study of larval settlement in the barnacle *Balanus amphitrite*. *PLoS One* 9, e88744. <https://doi.org/10.1371/journal.pone.0088744>.
17. Allocati, N., Masulli, M., Di Ilio, C., and Federici, L. (2018). Glutathione transferases: substrates, inhibitors and pro-drugs in cancer and neurodegenerative diseases. *Oncogenesis* 7, 8–15. <https://doi.org/10.1038/s41389-017-0025-3>.
18. Townsend, D.M., and Tew, K.D. (2003). The role of glutathione-S-transferase in anti-cancer drug resistance. *Oncogene* 22, 7369–7375. <https://doi.org/10.1038/sj.onc.1206940>.
19. Jancova, P., Anzenbacher, P., and Anzenbacherova, E. (2010). Phase II drug metabolizing enzymes. *Biomed. Pap. Med.*

- Fac. Univ. Palacky Olomouc Czech. Repub. 154, 103–116. <https://doi.org/10.5507/bp.2010.017>.
20. Anzenbacher, P., and Anzenbacherová, E. (2001). Cytochromes P450 and metabolism of xenobiotics. *Cell. Mol. Life Sci.* 58, 737–747. <https://doi.org/10.1007/pl00000897>.
 21. Yagishita, Y., Uruno, A., and Yamamoto, M. (2016). NRF2-mediated Gene Regulation and Glucose Homeostasis. *Mol Nutr Food Res (Academic Press)*, pp. 331–348. <https://doi.org/10.1016/B978-0-12-801585-8.00027-0>.
 22. Dubey, A., Prajapati, K.S., Swamy, M., and Pachauri, V. (2015). Heat shock proteins: a therapeutic target worth to consider. *Vet. World* 8, 46–51. <https://doi.org/10.14202/vetworld.2015.46-51>.
 23. Wang, K.L., Zhang, G., Sun, J., Xu, Y., Han, Z., Liu, L.L., Shao, C.L., Liu, Q.A., Wang, C.Y., and Qian, P.Y. (2016). Cochliomycin A inhibits the larval settlement of *Amphibalanus amphitrite* by activating the NO/cGMP pathway. *Biofouling* 32, 35–44. <https://doi.org/10.1080/08927014.2015.1121245>.
 24. Xu, Y., Zhang, L., Wang, K.L., Zhang, Y., and Wong, Y.H. (2020). Transcriptomic analysis of the mode of action of the candidate anti-fouling compound di (1H-indol-3-yl) methane (DIM) on a marine biofouling species, the bryozoan *Bugula neritina*. *Mar. Pollut. Bull.* 152, 110904. <https://doi.org/10.1016/j.marpolbul.2020.110904>.
 25. Chen, Z.F., Matsumura, K., Wang, H., Arellano, S.M., Yan, X., Alam, I., Archer, J.A.C., Bajic, V.B., and Qian, P.Y. (2011). Toward an understanding of the molecular mechanisms of barnacle larval settlement: a comparative transcriptomic approach. *PLoS One* 6, e22913. <https://doi.org/10.1371/journal.pone.0022913>.
 26. Deák, F., Anderson, R.E., Fessler, J.L., and Sherry, D.M. (2019). Novel cellular functions of very long chain-fatty acids: insight from ELOVL4 mutations. *Front. Cell. Neurosci.* 13, 428. <https://doi.org/10.3389/fncel.2019.00428>.
 27. Pamarthy, S., Kulshrestha, A., Katara, G.K., and Beaman, K.D. (2018). The curious case of vacuolar ATPase: regulation of signaling pathways. *Mol. Cancer* 17, 41. <https://doi.org/10.1186/s12943-018-0811-3>.
 28. She, W., Ye, W., Cheng, A., Liu, X., Tang, J., Lan, Y., Chen, F., and Qian, P.Y. (2021). Discovery, bioactivity evaluation, biosynthetic gene cluster identification, and heterologous expression of novel albolungin derivatives. *Front. Microbiol.* 12, 635268. <https://doi.org/10.3389/fmicb.2021.635268>.
 29. Freeman, J.A., and Costlow, J.D. (1983). The cyprid molt cycle and its hormonal control in the barnacle *Balanus amphitrite*. *J. Crustac Biol.* 3, 173–182. <https://doi.org/10.2307/1548253>.
 30. Fujii, T., Kakino, K., Tanaka, M., Lee, J.M., Kusakabe, T., and Banno, Y. (2020). A defect in purine nucleotide metabolism in the silkworm, *Bombyx mori*, causes a translucent larval integument and male infertility. *Insect Biochem. Mol. Biol.* 126, 103458. <https://doi.org/10.1016/j.ibmb.2020.103458>.
 31. Chen, Z.F., Wang, H., Matsumura, K., and Qian, P.Y. (2012). Expression of calmodulin and myosin light chain kinase during larval settlement of the barnacle *Balanus amphitrite*. *PLoS One* 7, e31337. <https://doi.org/10.1371/journal.pone.0031337>.
 32. Zhang, G., Wong, Y.H., Zhang, Y., He, L.S., Xu, Y., and Qian, P.Y. (2015). Nitric oxide inhibits larval settlement in *Amphibalanus amphitrite* cyprids by repressing muscle locomotion and molting. *Proteomics* 15, 3854–3864. <https://doi.org/10.1002/pmic.201500112>.
 33. Gallus, L., Ferrando, S., Gambardella, C., Faimali, M., Piazza, V., and Masini, M.A. (2013). Nitric oxide synthase (NOS) in the cyprid of *Amphibalanus amphitrite* (Cirripedia, Crustacea). *Neurosci. Lett.* 555, 209–214. <https://doi.org/10.1016/j.neulet.2013.09.041>.
 34. Piazza, M., Guillemette, J.G., and Dieckmann, T. (2015). Dynamics of nitric oxide synthase–calmodulin interactions at physiological calcium concentrations. *Biochemistry* 54, 1989–2000. <https://doi.org/10.1021/bi501353s>.
 35. Pronin, A.N., Satpaev, D.K., Slepak, V.Z., and Benovic, J.L. (1997). Regulation of G protein-coupled receptor kinases by calmodulin and localization of the calmodulin binding domain. *J. Biol. Chem.* 272, 18273–18280. <https://doi.org/10.1074/jbc.272.29.18273>.
 36. Swulius, M.T., and Waxham, M.N. (2008). Ca²⁺/calmodulin-dependent protein kinases. *Cell. Mol. Life Sci.* 65, 2637–2657. <https://doi.org/10.1007/s00018-008-8086-2>.
 37. Zhang, Y., He, L.S., Zhang, G., Xu, Y., Lee, O.O., Matsumura, K., and Qian, P.Y. (2012). The regulatory role of the NO/cGMP signal transduction cascade during larval attachment and metamorphosis of the barnacle *Balanus* (= *Amphibalanus*) *amphitrite*. *J. Exp. Biol.* 215, 3813–3822. <https://doi.org/10.1242/jeb.070235>.
 38. Haas, B.J., Papanicolaou, A., Yassour, M., Grabherr, M., Blood, P.D., Bowden, J., Couger, M.B., Eccles, D., Li, B., Lieber, M., et al. (2013). De novo transcript sequence reconstruction from RNA-seq using the Trinity platform for reference generation and analysis. *Nat. Protoc.* 8, 1494–1512. <https://doi.org/10.1038/nprot.2013.084>.
 39. Li, W., and Godzik, A. (2006). Cd-hit: a fast program for clustering and comparing large sets of protein or nucleotide sequences. *Bioinformatics* 22, 1658–1659. <https://doi.org/10.1093/bioinformatics/btl158>.
 40. Bolger, A.M., Lohse, M., and Usadel, B. (2014). Trimmomatic: a flexible trimmer for Illumina sequence data. *Bioinformatics* 30, 2114–2120. <https://doi.org/10.1093/bioinformatics/btu170>.
 41. Simão, F.A., Waterhouse, R.M., Ioannidis, P., Kriventseva, E.V., and Zdobnov, E.M. (2015). BUSCO: assessing genome assembly and annotation completeness with single-copy orthologs. *Bioinformatics* 31, 3210–3212. <https://doi.org/10.1093/bioinformatics/btv351>.
 42. Patro, R., Duggal, G., Love, M.I., Irizarry, R.A., and Kingsford, C. (2017). Salmon provides fast and bias-aware quantification of transcript expression. *Nat. Methods* 14, 417–419. <https://doi.org/10.1038/nmeth.4197>.
 43. Cantalapiedra, C.P., Hernández-Plaza, A., Letunic, I., Bork, P., and Huerta-Cepas, J. (2021). eggNOG-mapper v2: functional annotation, orthology assignments, and domain prediction at the metagenomic scale. *Mol. Biol. Evol.* 38, 5825–5829. <https://doi.org/10.1093/molbev/msab293>.
 44. Love, M.I., Huber, W., and Anders, S. (2014). Moderated estimation of fold change and dispersion for RNA-seq data with DESeq2. *Genome Biol.* 15, 550–621. <https://doi.org/10.1186/s13059-014-0550-8>.
 45. Meier, F., Brunner, A.D., Koch, S., Koch, H., Lubeck, M., Krause, M., Goedecke, N., Decker, J., Kosinski, T., Park, M.A., et al. (2018). Online parallel accumulation–serial fragmentation (PASEF) with a novel trapped ion mobility mass spectrometer. *Mol. Cell. Proteomics* 17, 2534–2545. <https://doi.org/10.1074/mcp.TIR118.000900>.
 46. Livak, K.J., and Schmittgen, T.D. (2001). Analysis of relative gene expression data using real-time quantitative PCR and the 2⁻(Delta Delta C(T)) Method. *Methods* 25, 402–408. <https://doi.org/10.1006/meth.2001.1262>.

STAR★METHODS

KEY RESOURCES TABLE

REAGENT or RESOURCE	SOURCE	IDENTIFIER
Chemicals, peptides, and recombinant proteins		
UltraPure™ SSC	Thermo Fisher	Cat#15557044
UltraPure™ Salmon Sperm DNA Solution	Thermo Fisher	Cat#15632011
Sheep Serum	Thermo Fisher	Cat#16070096
UltraPure™ 0.5 M EDTA (pH 8.0)	Thermo Fisher	Cat#15575020
Proteinase K Solution	Thermo Fisher	Cat#4333793
Alexa fluor™ 555 phalloidin	Thermo Fisher	Cat#A34055
Goat anti-Mouse IgG1 Cross-Adsorbed Secondary Antibody, Alexa Fluor™ 647	Thermo Fisher	Cat#A-21240
DAPI	Thermo Fisher	Cat#D21490
Concanavalin A, Alexa Fluor™ 488 Conjugate	Thermo Fisher	Cat#C11252
RNAlater™ Stabilization Solution	Thermo Fisher	Cat#AM7020
1-Step™ NBT/BCIP Substrate Solution	Thermo Fisher	Cat#34042
TWEEN 20	Sigma–Aldrich	CAS: 9005-64-5
Formamide	Sigma–Aldrich	CAS:75-12-7
Heparin sodium	Sigma–Aldrich	CAS:9041-08-1
Digoxigenin (DIG)	Sigma–Aldrich	CAS:1672-46-4
Bovine serum albumin (BSA)	Sigma–Aldrich	CAS:9048-46-8
Anti-Digoxigenin-AP, Fab fragments	Sigma–Aldrich	Cat#11093274910
Anti-acetylated tubulin antibody	Sigma–Aldrich	Cat#T7451
Critical commercial assays		
PreOmics iST-PreOn kit	PreOmics	Cat#P.O.00001
Bradford protein assay kit	Bio-Rad	Cat#5000001
RNeasy Micro Kit	QIAGEN	Cat#74004
HiScript III All-in-one RT SuperMix Perfect for qRT-PCR kit	Vazyme	Cat#R333-01
Deposited data		
Raw RNA-seq data of <i>Amphibalanus Amphitrite</i>	This study	BioProject: PRJNA917251
Mass spectrometry proteomics data submitted to ProteomeXchange	This study	ProteomeXchange: PXD039255
Software and algorithms		
Transdecoder v5.5.0	Haas et al., 2013 ³⁸	NA
CD-HIT-EST	Li and Godzik, 2006 ³⁹	NA
PEAKS Studio version X pro	Bioinformatics Solutions Inc.	NA
Trimmomatic version 0.39	Bolger et al., 2014 ⁴⁰	NA
BUSCO v4	Simão et al., 2015 ⁴¹	NA
Salmon v1.7.0	Patro et al., 2017 ⁴²	NA
eggNOG-mapper v2	Cantalapiedra et al., 2021 ⁴³	NA
DESeq2	Love et al., 2014 ⁴⁴	NA
OmicsBox version 1.4.11	Biobam	NA

RESOURCE AVAILABILITY

Lead contact

Further information and requests for resources and reagents should be directed to and will be fulfilled by the lead contact, Pei-Yuan Qian (boqianpy@ust.hk).

Materials availability

This study did not generate new unique reagents.

Data and code availability

- All data reported in this paper will be shared by the [lead contact](#) upon request.
- Raw *Amphibalanus amphitrite* RNA-seq data have been deposited at NCBI and are publicly available as of the date of publication. Accession numbers are listed in the [key resources table](#).
- Mass spectrometry proteomics data have been deposited at ProteomeXchange and are publicly available as of the date of publication. Accession numbers are listed in the [key resources table](#).
- This paper does not report original code.
- Any additional information required to reanalyze the data reported in this paper is available from the [lead contact](#) upon request.

EXPERIMENTAL MODEL AND SUBJECT DETAILS

Larval collection and culture

A. amphitrite adults were collected from Pak Sha Wan Pier, Hong Kong (22°38'N, 114°28'E) and kept in the dark for 24 hours. A light source (LED lamp, 1,500 lumens) was used to stimulate larval release. Within 1 hour, larvae were collected and cultured in 0.22 μm filtered seawater with a daily diet of *Chaetoceros gracilis* Schutt at 1×10^6 cells mL^{-1} until their growth into cyprids, which were used for anti-larval settlement bioassay.

METHOD DETAILS

Larval bioassays

The bioassay was conducted in a 24-well polystyrene tissue culture plate with 15–20 larvae in each well. About 0.1% of DMSO in filtered seawater (FSW) and 0.625, 1.25, 2.5, 5, 10, 20, and 40 $\mu\text{g mL}^{-1}$ albobungin were tested in triplicate. In each well, 1 mL of FSW containing 15–20 larvae and 1 mL of albobungin solution of different concentrations were added. The wells with 0.1% DMSO in FSW served as a negative control, and butenolide was used as a positive control. After incubation at 25°C for 48 hours, the number of attached, swimming, and dead larvae were counted under an Olympus optical microscope (Olympus Corporation, Tokyo, Japan). Settlement rate was calculated as the ratio of settled larvae to the total number of larvae in each well. Death rate was calculated as the ratio of dead or missing larvae to the total number of larvae in each well.

For the recovery assay, the larvae were treated with different concentrations of albobungin for 24 hours. Then the compound was removed by washing the larvae in filtered seawater three times. Each well was added with 1 mL of filtered seawater, and the plate was kept for another 24 hours. Settlement rate was calculated as the ratio of settled larvae to the total number of larvae in each well. Death rate was calculated as the ratio of dead or missing larvae to the total number of larvae in each well.

Sample preparation for proteomics

Around 500 cyprids larvae were treated with 5 $\mu\text{g mL}^{-1}$ albobungin in a 100 mm TC-treated culture dish for 24 hours to prepare larval samples for proteomics. The larvae kept in the FSW were used as a control group. Each treatment group and control group had four replicates. After 24 hours, unsettled swimming larvae were collected and washed for protein extraction. Briefly, the larvae were suspended in 300 μL of lysis buffer (8 M Urea, 50 mM Tris-HCl, pH=8.0) and sonicated for 15 minutes. The samples were centrifuged to remove cell debris. Protein concentration was measured by Bradford protein assay kit (Bio-Rad, Hercules, USA). After protein quantification, the cell pellet was further precipitated using four volumes of cool acetone overnight and centrifuged using 15,000 g for 30 minutes at 4°C. The dried pellets were digested and purified

using the PreOmics iST-PreOn kit (PreOmics, Planegg, Germany) on the automated PreON machine (PreOmics, Planegg, Germany). The purified samples were reconstituted in 0.1% formic acid in water with a final concentration of 200 ng μL^{-1} and 1 μL was injected into Bruker nanoElute ultrahigh-performance liquid chromatograph (UHPLC, Bruker Daltonics, Bremen, Germany) and separated on an IonOptiks 25 cm Aurora Series emitter column with CaptiveSpray insert (250 mm by 75 μm internal diameter, 120 \AA pore size, 1.6 μm particle size C18) at a flow rate of 0.3 $\mu\text{L min}^{-1}$ from 2% to 95% acetonitrile (mobile phases A and B) in 30 minutes. Mobile phase A is 2% acetonitrile (diluted in MilliQ Water) with 0.1% formic acid, and mobile phase B is 100% acetonitrile with 0.1% formic acid. For the Bruker TimsTOF Pro mass spectrometer (Bruker Headquarters Billerica, MA, United States), we recorded the mass spectra in the range from m/z 100 to 1700 by a positive electrospray mode. The scan range of ion mobility was from 0.85 to 1.30 Vs/ cm^2 , and the collision energy was linearly raised from 27 eV to 45 eV as a function of increasing ion mobility as previously reported.⁴⁵

RNA sample preparation and sequencing

Treated and untreated samples were prepared as described above for RNA sequencing. After the larvae were harvested, they were fixed and stored in an RNAlater solution until RNA extraction. The total RNA of *A. amphitrite* was extracted using an RNA extraction kit according to the manufacturer's protocol (QIAGEN, Hilden, Germany). The quantity and quality of the extracted RNA were measured by BioDrop (Biochrom, Cambridge, UK) and agarose gel electrophoresis. cDNA synthesis and eukaryotic library construction were conducted from each individual's mRNA enriched by oligo(dT) probes. A paired-end read with a length of 150 bp was generated by Illumina NovaSeq 6000 (Illumina, San Diego, CA, USA) in Novogene (Beijing, China) from each cDNA library. The data were deposited in the NCBI database (Table S1).

Transcriptome assembly and annotation

The low-quality reads and adaptors were trimmed by Trimmomatic version 0.39⁴⁰ with default settings: ILLUMINACLIP: TruSeq3-PE-2.fa:2:30:10 LEADING:10 TRAILING:10 SLIDINGWINDOW:4:18 MINLEN:40. The cleaned reads were mapped to the reference transcriptome (NCBI access number: PRJNA751628), and transcript expression levels were quantified using Salmon v1.7.0.⁴² BUSCO v4⁴¹ was used to evaluate the comprehensiveness of the *A. amphitrite* transcriptome assembly by searching against the metazoa_odb10 database.

The Kyoto Encyclopedia of Genes and Genomes (KEGG) database through the KEGG Automatic Annotation Server (KAAS), the Gene Ontology (GO) through OmicsBox version 1.4.11 (BioBam, Valencia, Spain), and the KOG through eggNOG-mapper v2⁴³ were enriched for further analysis to determine gene function.

qPCR analysis

The RNA samples were prepared using an RNA extraction kit according to the manufacturer's protocol (QIAGEN, Hilden, Germany). Then, the genomic DNA was removed and cDNA was synthesized using a Hi-Script III All-in-one RT SuperMix Perfect for qRT-PCR kit (Vazyme, Nanjing, China). The qPCR analysis was performed on Roche Diagnostics LightCycler 480 Instrument II Real-time PCR System using LightCycler® 480 SYBR Green I Master (Roche, Basel, Switzerland). The primers used are listed in Table S2. The cytochrome b (*cyt b*) was selected as the internal reference, and the relative expression level of each gene was normalized to *cyt b*.

In situ hybridization

A. amphitrite cyprids were collected, relaxed in 0.37 M MgCl_2 (1:1 mixed with filtered seawater) for 30 minutes, and fixed with fixation buffer (4% paraformaldehyde (PFA), autoclaved) at 4°C overnight. The samples for *in situ* hybridization were stored in methanol at -20°C before use. For immunofluorescence staining, the samples were washed with PBST (1X PBS, 0.1% Tween 20) three times to remove residual fixative and then permeabilized by treating in 20 $\mu\text{g mL}^{-1}$ proteinase K for 30 minutes at room temperature (RT). The samples were then fixed in 4% PFA for 30 minutes at RT and washed three times with PBST. The larvae were blocked in blocking buffer (2% BSA, 2% sheep serum, in PBST) for 1 hour at RT, incubated in Anti-Acetylated Tubulin antibody (1:1000 diluted in blocking buffer), and diluted Alexa fluorTM 555 conjugated phalloidin (1:250 diluted in blocking buffer) at 4°C overnight. The next day, the larvae were incubated in Alexa-fluorTM 647 conjugated goat-anti mouse IgG secondary antibody (1:1000 diluted in blocking buffer) for 2 hours at RT. After three PBST washes, the cell nuclei and plasma of the larvae were stained for

30 minutes at RT with 1:1000 diluted DAPI (diluted in PBST) and 1:200 diluted Alexa-fluor™ 488 Conjugate Concanavalin A (diluted in PBST), respectively. Finally, the larvae were washed three times in PBST, cleared in Murray's clear, and imaged by Zeiss LSM980 confocal microscope (Zeiss, Jena, Germany).

Whole mount *in situ* hybridization was performed using the protocol described before. The mRNA probe was synthesized and labeled with DIG. The primers used for synthesis of the mRNA probe are listed in Table S2. Briefly, the samples were rehydrated by successive dilution of methanol in PBST, three times in PBST, permeabilized with 20 $\mu\text{g mL}^{-1}$ proteinase K at 37°C for 30 minutes, and sonicated for 5 seconds. Then, the samples were fixed with 4% PFA for 30 minutes at RT and washed three times with PBST. The samples were pre-hybridized at 56°C for 1 hour in the hybridization mixture (50% formamide, 5 \times SSC, 0.1% Tween 20, 50 $\mu\text{g mL}^{-1}$ heparin, 500 $\mu\text{g mL}^{-1}$ salmon sperm DNA). Hybridization was performed in 200 μL of hybridization mixture containing 200 ng of antisense DIG-labeled RNA probe at 56°C overnight. The samples were washed three times in the PBST and blocked in 2% sheep serum, 2% BSA, and 1/10000 anti-DIG-AP in PBST at room temperature and 4°C overnight. The samples were washed five times in PBST and incubated in alkaline tris buffer (100 mM Tris-HCl, pH 9.5, 50 mM MgCl_2 , 100 mM NaCl, 0.1% Tween 20). The alkaline tris buffer was removed and replaced with an NBT/BCIP solution in darkness overnight. The samples were washed with the stop solution (1mM EDTA, PBST), mounted with 100% glycerol, observed under Olympus BX51 Microscope with DIC setting (Olympus, Tokyo, Japan), and photographed.

QUANTIFICATION AND STATISTICAL ANALYSIS

Database searching and label-free quantification (LFQ) of proteomics data

The transcriptome sequence of *A. amphitrite* (NCBI access number: PRJNA751628) was converted into a protein database by using Transdecoder v5.5.0³⁸ and CD-HIT-EST³⁹ to reduce redundant sequences with a threshold of 90% similarity. The raw data were converted into MGF format files and processed database search using PEAKS Studio version X pro. The parameters were 15.0 ppm parent mass error tolerance, 0.05 Da fragment mass error tolerance, and monoisotopic type. Only the proteins and peptides with false discovery rate (FDR) < 1% were filtered. A protein was considered differentially expressed if its fold change was higher or lower than two fold and the permutation-based FDR was less than 0.05. The ratio of the LFQ intensity value of the experimental and control groups was transformed to the \log_2 form. Two-tailed Student's t-test was used for statistical calculations.

Gene expression and enrichment analysis

The unigene expression level was expressed in transcripts per million (TPM). Differential expression and principal component (PCA) analyses were performed using DESeq2.⁴⁴ Differentially expressed genes were identified with threshold $\text{FDR} \leq 0.05$ and $|\log_2\text{Fold Change}| \geq 1$. For the enrichment analysis, the KEGG pathways were enriched through cumulative hypergeometric distribution by the OmicShare online tool (<https://www.omicshare.com/>).

Quantification of gene expression level from qPCR

For qPCR analysis, triplicates were repeated for each gene, and the relative gene expression level was calculated using the $2^{-\Delta\Delta\text{Ct}}$ method.⁴⁶

Statistical analysis

Experiments were performed in three independent batches of larvae. Data were analyzed by one-way ANOVA to detect significant differences in the larval settlement, and SD was calculated by GraphPad Prism 9.